05,12

Magnetic properties of nanocrystalline material based on $Bi_2Fe_4O_9$

© I.V. Buryanenko[1], V.G. Semenov[2,3], N.A. Lomanova[4,¶], A.V. Osipov[5], M.P. Volkov[4], I.V. Pleshakov[4]

[1] Peter the Great Saint-Petersburg Polytechnic University,
St. Petersburg, Russia
[2] St. Petersburg State University,
St. Petersburg, Russia
[3] Institute for Analytical Instrumentation, Russian Academy of Sciences,
St. Petersburg, Russia
[4] Ioffe Institute,
St. Petersburg, Russia
[5] Grebenschikov Institute of Silicate Chemistry RAS,
St. Petersburg, Russia

¶ E-mail: natus@mail.ioffe.ru

Received January 12, 2022
Revised January 12, 2022
Accepted January 13, 2022

The magnetic characteristics of a nanocrystalline material based on bismuth ferrite $Bi_2Fe_4O_9$ with 60 ± 3 nm crystallites were studied. The obtained material demonstrates unusual magnetic properties, which are manifested in a significant increase in the value of magnetization in comparison with the data known from other works.

Keywords: nanocrystals, bismuth ferrite, mullite, magnetic properties.

DOI: 10.21883/PSS.2022.05.53513.274

1. Introduction

The interest in $Bi_2Fe_4O_9$ (bismuth ferrite) based materials with mullite-like structure is driven by their capability to be used in magnetoelectronics as multiferroics near room temperature [1,2], as gas sensor materials [3] and photocatalysts [4].

$Bi_2Fe_4O_9$ has a rhombic lattice cell (space group pbam) with $a = 7.9$ Å, $b = 8.4$ Å and $c = 6.0$ Å ($Z = 2$) where iron atoms are localized in FeO_6 oxygen octahedra and FeO_4 tetrahedra [5]. Iron spins have a ferromagnetic type interaction in octahedra and antiferromagnetic coupling between each other and octahedral iron spins in tetrahedra [6,7]. Below room temperature, bulk $Bi_2Fe_4O_9$ is an antiferromagnetic with Neel point $T_N = 237-265$ K [7,8].

Ceramic samples show the presence of impurity phases that may influence the material's magnetic behavior [8–10]. In [8], it was found that $Bi_2Fe_4O_9$ is characterized by collinear ferromagnetic (FM) and noncollinear flat antiferromagnetic (AFM) spin ordering. It was shown that the appearance of non-zero magnetization (about $3\,\mu_B$/unit) of $Bi_2Fe_4O_9$ antiferromagnetic may be attributed to the presence of vacancies in the bismuth sublattice.

A solution combustion method is advantageous for production of nanocrystalline ferrites with various compositions, including $Bi_2Fe_4O_9$, at rather high temperature, since a fast combustion reaction process does not contribute to recrystallization particle growth [11–22].

Nanocrystalline $Bi_2Fe_4O_9$ particles smaller than 60 nm have a low magnetic moment whose occurrence is associated with the substance surface condition. Many publications report the probability of magnetization of $Bi_2Fe_4O_9$-based nanocrystalline materials near room temperature, but it is rather low [1,4,7,22]. (Some increase in magnetization is observed in $Bi_{2-x}A_xFe_4O_9$ type solid solutions due to iron ion redistribution in the structure [23]).

Mössbauer measurements of the iron ion states in complex oxides, including nanocrystalline ones, provide useful information about formation mechanisms and magnetic behavior of complex oxides [1,7,12,13,15–17,24–27]. Such experiments described in [1,7,17,27] have shown that the properties of $Bi_2Fe_4O_9$-based nanomaterials may differ greatly from the bulk substance properties. Therefore, it is desirable to further study the factors that enable to modify magnetic properties of $Bi_2Fe_4O_9$ nanocrystalline particles.

The purpose of this work was to study the magnetic characteristics of the $Bi_2Fe_4O_9$-based nanocrystalline material obtained by glycine-nitrate combustion method.

2. Experimental

The material was synthesized by the glycine-nitrate combustion method using bismuth nitrate, ferrous nitrate and glycine as precursors. Molar quantity ratio of glycine G and nitrate ions N was $G/N = 0.28$ which corresponded to the combustion reaction with 50% lack of glycine to ensure potential combustion temperature decrease and to achieve the target product with the smallest crystal size.

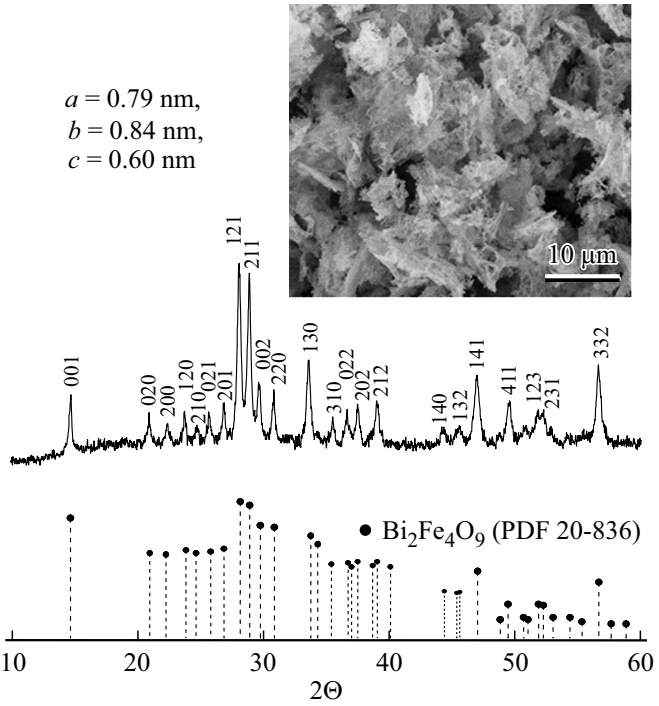

Figure 1. Diffraction pattern of $Bi_2Fe_4O_9$-based material (the detail shows a SEM-image of the sample).

Combustion product in the form brown powder was gradually heat treated at 350, 550 and 650°C during 20 min. After completion of the final synthesis stage at 650°C, the X-ray diffraction analysis data (XRD-7000 Shimadzu diffractometer, CuKα-radiation) showed the absence of appreciable amounts of bulk impurity phases (Fig. 1) and the main phase lattice cell parameters corresponded to $Bi_2Fe_4O_9$ (PDF 20-836). The average size of the target product crystallites calculated using the Scherrer equation is equal to 60 ± 3 nm.

Microstructure and elemental composition of the final material were measured by the scanning electron microscopy and energy dispersive spectroscopy methods (FEI Quanta 200 scanning election microscope with EDAX accessory). It has been found that the material consisted of porous particle aggregates (Fig. 1, detail). Average element ratio in the sample was Bi : Fe = 2.04 : 3.96, i.e. met the target stoichiometry within the method error.

Magnetic measurements were carried out using PPMS (Quantum Design) vibrating magnetometer. Dependences of specific magnetization M on field H in the temperature range from helium temperature to above room temperature as wells as temperature trend M at constant field $H = 200$ Oe in FC (field cooling) and ZFC (zero field cooling) conditions were investigated.

Mössbauer measurements of the samples were carried out using WISSEL spectrometer in adsorption geometry at room temperature (source — ^{57}Co in rhodium matrix, isomer shifts IS are given with respect to IS α-Fe).

Table 1. Magnetic properties of the sample

Temperature, K	H_c, kOe	M_r, emu/g	M, emu/g (20 kOe)	
			experiment*	publications**
5	3.5	1.65	3.14	–
100	1.3	0.92	2.97	–
200	0.54	0.54	2.76	–
300	0.23	0.27	2.40	0.5 [1]; 1.1 [7]
400	0.10	0.12	2.00	–

Note.
* Experimental data for a sample with a crystallite size of 60 nm;
** Data for samples with crystallite sizes 60–70 nm.

3. Magnetic measurement results

3.1. Magnetic measurements

$Bi_2Fe_4O_9$ magnetization loops measured at different temperatures are shown in Fig. 2. These curves significantly differ from the curves of ceramic and nanocrystalline samples synthesized in various conditions [1,2,7,8]. First of all, it shall be noted that the material shows an unusually high magnetization that substantially exceeds the values specified, for example, in [1,7] (see Table 1). M cannot be measured in saturation state because the latter is not achieved even at very high H as shown in Fig. 2. Magnetization reversal causes hysteresis which is specifically pronounced at low temperatures (Table 1). Curves $M(H)$ show a break that is common to magnetic-ordered materials and the similarity is maintained in the range $-140 < H < 140$ kOe up to $T = 400$ K.

Measurements of $M(T)$ in FC and ZFC conditions are shown in Fig. 3. These dependences are generally similar to those observed in most magnetic nanopowders. Divergence of the curves takes place at about 400 K with typical maxima (at $T > 200$ K) manifested poorly and smeared.

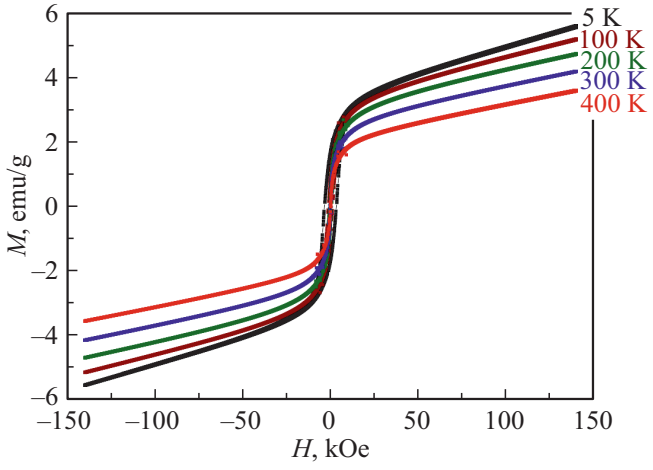

Figure 2. Sample magnetization curves measured at different temperatures.

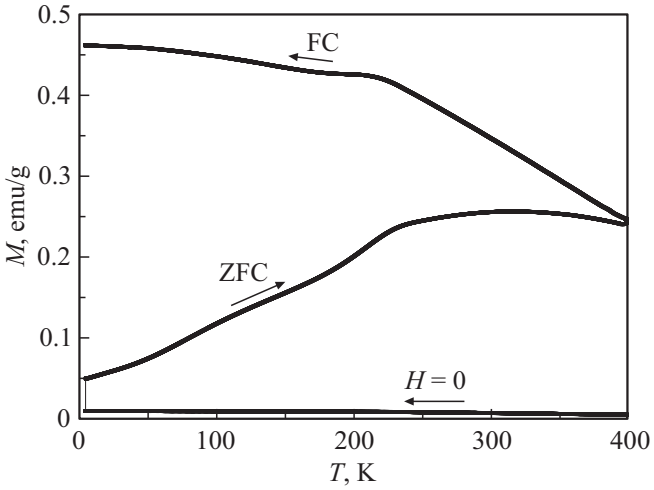

Figure 3. Temperature dependences FC/ZFC of the sample's specific magnetization measured at $H = 200$ Oe.

It shall be noted that an additional maximum at $T \approx 100$K can be identified at least on ZFC-curve.

3.2. Mössbauer spectroscopy

Mössbauer spectrum in Fig. 4 shows that the obtained material is paramagnetic at room temperature. The main spectrum segment is described by two doublets whose parameters are close to $Bi_2Fe_4O_9$ parameters known from publications [17,27]. Isomer shift IS and quadrupolar splitting $QS = 0.99$ and 0.42 mm/s are typical of Fe^{3+} ions in tetrahedral and octahedral environment, respectively (Table 2). The spectrum also shows a faint sextet whose parameters correspond to α-Fe_2O_3 which was not recorded by the X-ray diffractometry method in a form of bulk phase. It shall be noted that main reflection (104) of α-Fe_2O_3 (PDF 1-1053) can superimpose reflection (130) of $Bi_2Fe_4O_9$ (PDF 20-836) and they could be hard to distinguish by the X-ray method.

Table 2. Mössbauer spectrum parameters

Component	Γ, mm/s	*IS*, mm/s	*QS*, mm/s	H_{eff}, T	A, %
Doublet 1	–	0.24	0.99	–	39
Doublet 2	–	0.36	0.42	–	41
Sextet	1.48	0.34	0.08	44.7	20
	0.35*	0.39*	−0.16*	51.2*	–

Note. * α-Fe_2O_3 [28] parameters.

4. Discussion

Occurrence in the sample of α-Fe_2O_3 type phase that was found during Mössbauer measurements can be attributed to lower mixture combustion temperature in case of lack of organic fuel which also involves the presence of X-ray amorphous bismuth oxide that generally is localized at grain boundaries. Some reduction of hyperfine field $H_{eff} = 44$ T ($H_{eff} \approx 51$ T for crystalline phase) and wide width of line $\Gamma = 1.48$ mm/s (for crystalline phase $\Gamma \sim 0.3$ mm/s) show

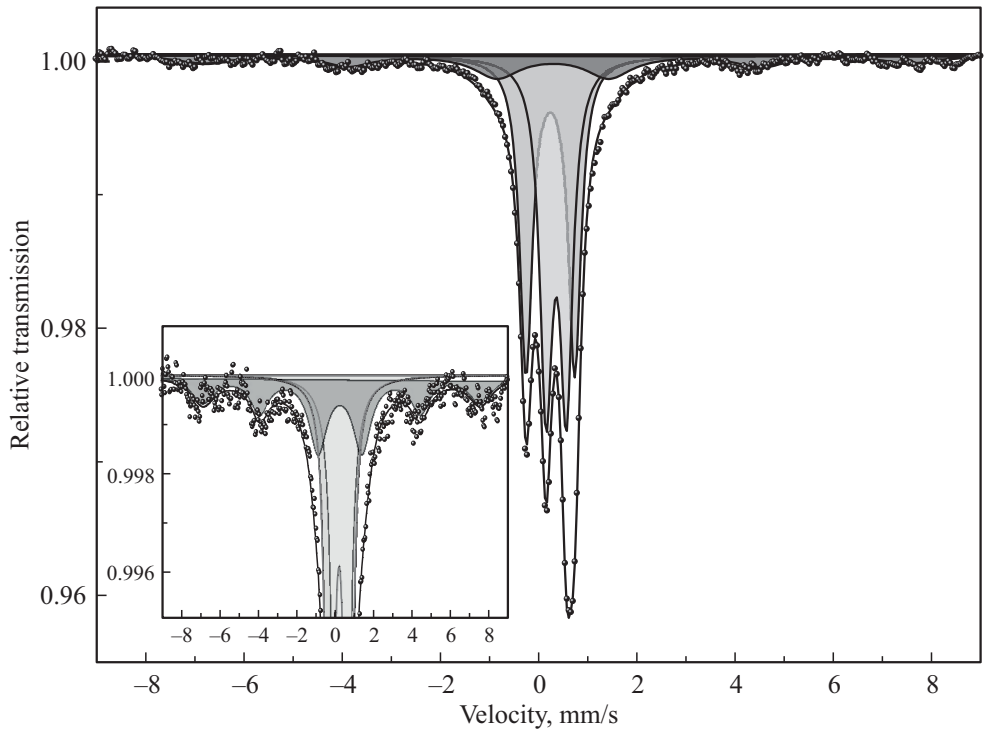

Figure 4. Mössbauer spectrum of $Bi_2Fe_4O_9$-based material (the detail shows a scaled-up spectrum segment).

that the hematite-like phase is nanodispersed. According to [13,16], small iron-containing clusters that have formed in similar synthesis conditions may be localized in closed pores, at grain boundaries and on nanocrystal surfaces. In [13,16,24], among potential processes that account for dramatic increase in magnetization of such materials, a surface effect inherent to nanoparticles is reported.

QS is indicative of iron ion environment asymmetry. Presence of α-Fe_2O_3 in $Bi_2Fe_4O_9$-based materials may have remained unnoticed in some publications [27] due to a narrower Mössbauer spectrum measurement range. In [17,20], such materials are reported to have some amount of iron-containing and bismuth-enriched bulk impurity phases.

Unusual magnetic properties of the material synthesized herein shall be probably attributed to the presence on the surface of $Bi_2Fe_4O_9$ nanocrystals of a hematite-like magnetic-ordered substance. High magnetization could have been hardly attributed only to the presence of an additional phase which exactly corresponds to α-Fe_2O_3 — in terms of magnetic properties, this crystalline oxide is an antiferromagnetic with low ferromagnetism and its trace amount in the sample could not have contributed significantly to the magnetic response. The foregoing, however, is indicative of the fact that its structure is heavily distorted. The presence of significant magnetization suggests that the low-ferromagnetic order is disturbed and α-Fe_2O_3 acquires a high total moment as a result of change in the antiparallel orientation of sublattice moments. Interaction with the main substance in the subsurface region may result in magnetic layer thickening and additional increase in the total magnetization. Such behavior is evidenced by gradual growth of M with increase in H — disoriented moments probably rotate in large fields (Fig. 2). In small fields, the system behaves as a supermagnetic with several magnetic fractions which may be seen from the data shown in Fig. 3.

Qualitatively similar behavior of magnetization curves up to $T = 400\,\mathrm{K}$ (Fig. 2) means that the magnetic order is maintained at least up to this temperature. At the same time, Mössbauer experiment shows that the main substance in the nanocristallite core is in paramagnetic state at room temperature (this is compliant with the known Neel point data). However, the paramagnetic response whose contribution (according to the assessment made for Fe^{3+} ions with frozen orbital moment and total moment $J = 5/2$) at $T > 260\,\mathrm{K}$ shall be rather high is not observed (this effect is indirectly reported in other publications [1]). Most likely, this can be attributed to the assumption that a magnetic-ordered shell formed at particle boundaries and consisting both of a hematite-like phase and probably of the adjacent layers with induced magnetism is rather thick and provides magnetic shielding of the core.

5. Conclusion

The glycine-nitrate combustion method was used to synthesize nanocrystalline $Bi_2Fe_4O_9$ material with an average crystallite size of $60 \pm 3\,\mathrm{nm}$ which has much higher magnetization (compared with that known from publications), and this substance is characterized by at least partial maintenance of magnetic-ordered state up to high temperatures ($400\,\mathrm{K}$). These unusual magnetic properties are presumably associated with occurrence of a surface layer in nanocrystals attributed to synthesis features and essentially responsible for magnetic characteristics of the system.

The findings may be useful for the development of new magnetic materials for magnetoelectronic application.

Acknowledgments

The authors are grateful to V.V. Gusarov (Ioffe Institute) for discussion of the findings and valuable comments.

Conflict of interest

The authors declare that they have no conflict of interest.

References

[1] Z.M. Tian, S.L. Yuan, X.L. Wang, X.F. Zheng, S.Y. Yin, C.H. Wang, L. Liu. J. Appl. Phys. **106**, 103912 (2009). http://dx.doi.org/10.1063/1.3259392
[2] X.H. Wu, J. Miao, Y. Zhao, X.B. Meng, X.G. Xu, S.G. Wang, Y. Jiang. Optoelectron. Adv. Mater. Rapid Commun. **7**, *1–2*, 116–120 (2013).
[3] J. Yang, J. Gao, P. Fu, Zh. Chen, Sh. Wang, L. Liu, Zh. Lin. Mater. Res. Express **6**, 095083 (2019).
[4] Q. Zhang, W. Gong, J. Wang, X. Ning, Zh. Wang, X. Zhao, W. Ren, Zh. Zhang. J. Phys. Chem. C **115**, 25241 (2011).
[5] Q. Zhang, P. Kong, H. Zhao, X. Shen, Y. Li, X. Li, J. Liu, C. Jin, R. Yu. High. Press. Res. **33**, 745 (2013).
[6] Z. Pchelkina, S. Streltsov. Phys. Rev. B **88**, 054424 (2013).
[7] S.A.N.H. Lavasani, O. Mirzaee, H. Shokrollahi, A.K. Moghadam, M. Salami. Ceram. Int. **43**, *15*, 12120 (2017).
[8] K. Jindal, Sh. Ameer, M. Tomar, P.K. Jha, V. Gupta. Materials Today: Proceed. **47**, *8*, 1637 (2021).
[9] M.N. Iliev, A.P. Litvinchuk, V.G. Hadjiev, M.M. Gospodinov, V. Skumryev, E. Ressouche. Phys. Rev. B **81**, 024302 (2010).
[10] A.K. Singh, S.D. Kaushik, B. Kumar, P.K. Mishra, A. Venimadhav, V. Siruguri, S. Patnaik. Appl. Phys. Lett. **92**, 132910 (2008).
[11] I.V. Pleshakov, M.P. Volkov, N.A. Lomanova, Yu.I. Kuzmin, V.V. Gusarov. Pis'ma v ZhTF **46**, *21*, 25 (2020). (in Russian)
[12] K.D. Martinson, V.A. Ivanov, M.I. Chebanenko, V.V. Panchuk, V.G. Semenov, V.I. Popkov. Nanosyst. Phys. Chem. Math. **10**, *6*, 694 (2019).
[13] N.A. Lomanova, M.V. Tomkovich, D.P. Danilovich, A.V. Osipov, V.V. Panchuk, V.G. Semenov, I.V. Pleshakov, M.P. Volkov, V.V. Gusarov. Neorgan. materialy **56**, *12*, 1342 (2020) (in Russian).
[14] K.D. Martinson, V.I. Popkov. Nanosyst. Phys. Chem. Math. **12**, *5*, 634 (2021).
[15] V.I. Popkov, K.D. Martinson, I.S. Kondrashkova, M.O. Enikeeva, V.N. Nevedomskiy, V.V. Panchuk, V.G. Semenov, M.P. Volkov, I.V. Pleshakov. J. Alloy. Compd. **859**, ArtNo 157812 (2021).

[16] N.A. Lomanova, V.V. Panchuk, V.G. Semenov, I.V. Pleshakov, M.P. Volkov, V.V. Gusarov. Ferroelectrics **569**, *1*, 240 (2020).
[17] A. Panda, R. Govindaraj, K. Vinod, G. Amarendr. AIP Conf. Proceed. **1953**, 120058 (2018).
[18] O.N. Karpov, M.V. Tomkovich, E.A. Tugova. Zhurn. obshch. khimii **88**, *10*, 1692 (2018) (in Russian).
[19] J. Zhao, T. Liu, Y. Xu, Y. He, W. Chen. Mater. Chem. Phys. **128**, 388 (2011).
[20] E. Tugova, S. Yastrebov, O. Karpov, R. Smith. J. Cryst. Growth **467**, 88 (2017).
[21] E.A. Tugova, O.N. Karpov. Rare Met. **40**, *7*, 1778 (2021).
[22] K.D. Martinson, V.A. Ivanov, M.I. Chebanenko, V.V. Panchuk, V.G. Semenov, V.I. Popkov. Nanosyst. Phys. Chem. Math. **10**, *6*, 694 (2019).
[23] Y.Y. Liang, J.X. Lei, X.X. Wang, L.G. Wang, C.M. Zhu. J. Mater. Sci.: Mater. Electron. **30**, 1691 (2019).
[24] T.-J. Park, G.C. Papaefthymiou, A.J. Viescas, A.R. Moodenbaugh, S.S. Wong. Nano Lett. **7**, 766 (2007).
[25] E.A. Tugova, A.A. Krasilin, V.V. Panchuk, V.G. Semenov, V.V. Gusarov. Ceram. Int. **46**, *15*, 24526 (2020).
[26] O.V. Proskurina, R.S. Abiev, D.P. Danilovich, V.V. Panchuk, V.G. Semenov, V.N. Nevedomsky, V.V. Gusarov. Chem. Eng. Proc. — Proc. Intensif. **143**, 107598 (2019).
[27] A. Kirsch, M.M. Murshed, P. Gaczynski, K.-D. Becker, Th.M. Gesing. Z. Naturforsch. **71**, *5*, 447 (2016).
[28] I.S. Lyubutin, C.R. Lin, Yu.V. Korzhetskiy, T.V. Dmitrieva, R.K. Chiang. J. Appl. Phys. **106**, 034311 (2009).